

Dynamics and stability of contractile actomyosin ring in the cell

Mainak Chatterjee, Arkya Chatterjee¹, Amitabha Nandi, and Anirban Sain²

Department of Physics, Indian Institute of Technology-Bombay, Powai, Mumbai 400076, India

(Dated: January 26, 2022)

Contraction of the cytokinetic ring during cell division leads to physical partitioning of a eukaryotic cell into two daughter cells. This involves flows of actin filaments and myosin motors in the growing membrane interface at the mid-plane of the dividing cell. Assuming boundary driven alignment of the acto-myosin filaments at the inner edge of the interface we explore how the resulting active stresses influence the flow. Using the continuum gel theory framework, we obtain exact axisymmetric solutions of the dynamical equations. These solutions are consistent with experimental observations on closure rate. Using these solutions we perform linear stability analysis for the contracting ring under non-axisymmetric deformations. Our analysis shows that few low wave number modes, which are unstable during onset of the constriction, later on become stable when the ring shrinks to smaller radii, which is a generic feature of actomyosin ring closure. Our theory also captures how the effective tension in the ring decreases with its radius causing significant slow down in the contraction process at later times.

PACS numbers: 87.16.Ka, 87.16.ad, 87.16.dj, 87.17.Ee

Cell division is fundamental to all living organisms. The last stage of cell division is called cytokinesis, where closure of a polymeric ring, made of actin filaments and myosin molecular motors [1, 2] completes the physical partitioning of the cell. In one mode of partitioning an intercellular membrane forms (see Fig-1a). This is common in mitotic cell divisions (eg., in *C. elegans* embryo, a widely studied model system for eukaryotes) and also in some compact tissues [3]. In the other mode (see Fig-1b), the contact area between the daughter cells gradually shrinks to zero, as the division furrow (the cusp in Fig-1b) caves in [4]. Here we focus on the development of the intercellular membrane (the first mode) which starts out as an annulus at the equatorial plane (see Fig-1a and inset-c) and gradually closes itself, as its inner boundary grows radially inward. The growth is assisted by the flow of actomyosin, beneath the cell surface (*the cortical flow*) [5]. Experiments suggest [1, 2, 6] that the ATP driven interaction between actin and myosin lead to the generation of *active* contractile stresses in the cytokinetic ring. How this stress changes with time during the course of the constriction however is not clear. Earlier models [4, 7] explain the observed contraction rate by assuming a constant contractile stress. Ref [8] had in addition assumed, an adhoc intrinsic dynamic friction, to account for the eventual slowdown of the contraction process.

Such an approach, that considers the actin ring to be a separate entity attached with the growing active membrane, cannot explain the recent experimental observations [9] where the ring is found to reorganize and constrict even after part of it is destroyed by localized laser ablation. This motivates us to consider the cortical ring to be part of the acto-myosin continuum spread over the growing membrane interface. In Ref [10], the authors developed an active gel model of the cytoskeletal flows to discuss wound healing in *Xenopus* oocyte [11]. Such a description involves solution of coupled equations for

the actin alignment field $Q_{\alpha\beta}(r)$ (the order parameter OP) and the velocity field $v_{\alpha}(r)$. The ring was assumed to be a narrow annular zone with higher level of myosin activity $\zeta\Delta\mu$ than the rest of the growing interface.

In this Letter, we follow a similar continuum gel theory approach and first solve the coupled equations for the OP and the velocity fields numerically (Fig-1), retaining flow coupling. But instead of assuming an active contractility gradient, which is standard in the literature [10], we use the observation, that actin filaments are aligned tangentially to the inner boundary of the closing annulus [12, 13], as a boundary condition. This is motivated by recent experiments [14, 15] which indicate that local assembly kinetics, like guided polymerization, can drive rapid filament alignment at the ring, at a much faster rate compared to the relatively slow hydrodynamic modes of the OP and the flow fields. The mean (time averaged) effect of this molecular level, fast, alignment kinetics can be incorporated in the hydrodynamic equation for the OP field as a boundary condition. Such a boundary driven alignment was used in Ref[16?] to solve for the OP field. Ref[16] reported that acto-myosin filaments at open cell boundaries can respond to the curvature of the boundary, and align parallel or perpendicular to the concave or convex boundaries, respectively. Encouraged by these observations, on boundary driven alignment, we set out to compute, a) the constriction rate of the cytokinetic ring, and b) its stability with respect to non-axisymmetric deformations, which has wide applicability across eukaryotic cell division.

Model: The actomyosin gel on the growing interface is modeled as a nematic fluid. Orientational order in a nematic fluid, in 3-dimensions, is defined by the tensor order parameter $Q_{\alpha\beta} = \langle n_{\alpha}n_{\beta} - \delta_{\alpha\beta}/3 \rangle$, where n_{α} is the nematic director field, and $\alpha, \beta = (x, y, z)$. As the acto-myosin filaments (nematic directors) lie in the flat interface $(x - y)$, symmetry and tracelessness of $Q_{\alpha\beta}$

dictate that the non-diagonal matrix elements involving z are zero, $Q_{xy} = Q_{yx} = q$, $Q_{zz} = -1/3$, and $Q_{xx} + Q_{yy} = 1/3$. Further, if the orientation distribution is isotropic in the $x - y$ plane then the resulting matrix $Q_{\alpha\beta}^0$ is diagonal, with $Q_{xx}^0 = Q_{yy}^0 = 1/6$, and $Q_{zz}^0 = -1/3$. In the presence of cortical flows or due to specific boundary conditions the isotropic distribution is modified to $Q_{\alpha\beta} = Q_{\alpha\beta}^0 + Q'_{\alpha\beta}$. Again symmetric structure and tracelessness of $Q_{\alpha\beta}$ require (see Supplementary information -SI) that, $Q'_{xx} = -Q'_{yy} = \tilde{Q}$, $Q'_{xy} = Q'_{yx} = q$, and rest of the elements are zero. This form remains invariant as we transform from cartesian to 2D polar coordinates later.

Active gel model for acto-myosin filaments : The free energy of the inhomogeneous nematic field can be described by the Landau-De Gennes form [17], using the Q' matrix. $\mathcal{F} = \int d^3r \left(\frac{\chi}{2} Q'_{ij} Q'_{ji} + \frac{L}{2} \partial_k Q'_{ij} \partial_k Q'_{ij} \right)$. This enforces an isotropic arrangement of the director field in the bulk of the 2D growing cortical layer with a correlation length $L_c = \sqrt{L/\chi}$. Later, we will see that this turns out to be the width of the actomyosin ring, which has been measured [18] to be $\sim 1\mu m$.

Constitutive equations of the active gel can be described by a linear relationship between thermodynamic fluxes and forces [10, 19–21]. We choose stress tensor $\sigma_{\alpha\beta}$, the rate of change of nematic order parameter $\frac{DQ_{\alpha\beta}}{Dt}$, and the rate of ATP consumption as the fluxes. The conjugate forces are the strain rate $v_{\alpha\beta} = \frac{1}{2}(\partial_\alpha v_\beta + \partial_\beta v_\alpha)$, the traceless nematic force field $H_{\alpha\beta} = -\frac{\delta\mathcal{F}}{\delta Q'_{\alpha\beta}}$, and the chemical potential difference generated due to ATP hydrolysis $\Delta\mu$. Following [10] the hydrodynamic equations in the liquid limit can be expressed as follows:

$$\sigma_{\alpha\beta} = 2\eta v_{\alpha\beta} - \beta_1 H_{\alpha\beta} + \zeta \Delta\mu Q_{\alpha\beta}, \quad (1)$$

$$\frac{D}{Dt} Q_{\alpha\beta} = \beta_1 v_{\alpha\beta} + \frac{1}{\beta_2} H_{\alpha\beta}. \quad (2)$$

$\frac{D}{Dt}$ here implies material derivative [19], $\zeta \Delta\mu Q_{\alpha\beta}$ is the active stress and contractility of the cortical layer enforces $\zeta > 0$ [19, 20]. We ignored any explicit active term in the second equation because it just renormalizes the inverse susceptibility χ^{-1} . Here η is the fluid viscosity while β_1 and β_2 are Onsager coefficients [10], and give the flow coupling and nematic relaxation strengths, respectively [10].

Following [10], we define a 2D ‘‘tension tensor’’ t_{ij} via the relation $t_{ij} = \int (\sigma_{ij} - \delta_{ij} P) dz$. Imposing the net normal stress on the interface t_{zz} to be zero yields pressure $P = \sigma_{zz}$. Further, ignoring variation of stress across the thin interface, we get [10] $t_{ij} = e(\sigma_{ij} - \delta_{ij} \sigma_{zz})$, where e is the effective thickness of the interface, assumed to be a constant here. This tension tensor allows us to write a two-dimensional hydrodynamic theory with the force balance equation as $\frac{\partial}{\partial t}(\rho v_i) = \partial_j t_{ij} - \alpha v_i$. Here α is the cytoplasmic friction external to the growing membrane interface. The flat growing interface has an annu-

lar shape, see inset of Fig.1c. The shrinking cytokinetic ring of radius $R_0(t)$ lies at its inner periphery, while its outer periphery is fixed at radius r_0 . After changing to 2D polar co-ordinates, and dropping the time derivative in highly viscous regime, the force balance equations are $\partial_r t_{rr} + \frac{1}{r}(t_{rr} - t_{\theta\theta}) + \frac{1}{r} \partial_\theta t_{r\theta} = \alpha v_r$, and $\partial_r t_{\theta r} + \frac{1}{r}(t_{\theta r} + t_{r\theta}) + \frac{1}{r} \partial_\theta t_{\theta\theta} = \alpha v_\theta$ (see SI).

The 2×2 (xy) block of $Q'_{\alpha\beta}$ matrix (anisotropic part) remains traceless and symmetric, parameterised by two variables \tilde{Q} and q , although their values change in the polar frame. The 2×2 block of the isotropic matrix however remains unchanged, $Q_{\alpha\beta}^0 = \mathbb{I}/6$, where \mathbb{I} is the identity matrix (see SI).

Rotationally symmetric solutions for $Q'_{\alpha\beta}(r)$ and $v_\alpha(r)$: We first consider the special case where the circular ring is at $r = R_0$, with our domain of interest $r \geq R_0$. We start with $\alpha = 0$, set stress free boundary condition at the open edge, i.e., normal stress $\sigma_{rr}(R_0) = 0$, and $v_r = 0$ at $r \rightarrow \infty$. The nematic directors are assumed to be parallel to the inner boundary, i.e., $\hat{n}(R_0) = \hat{\theta}$, and isotropic as $r \rightarrow \infty$. It implies, that at $r = R_0$, the anisotropic $Q'_{\alpha\beta}$ matrix is diagonal with $Q'_{rr} = -Q'_{\theta\theta} = \tilde{Q} = -1/2$ (see SI), and $Q'_{\alpha\beta}(r = \infty) = 0$.

We assume a quasi-steady state where the material derivative $DQ_{\alpha\beta}/Dt = 0$ in Eq.2. Note that $\partial Q_{\alpha\beta}/\partial t \neq 0$ since the inner edge R_0 keeps moving, but the convection term $\mathbf{v} \cdot \nabla Q_{\alpha\beta}$ counters this change to keep $Q_{\alpha\beta}$ unaltered in the material frame. This yields $H_{\alpha\beta} = -\beta_1 \beta_2 v_{\alpha\beta}$. When expressed in polar form the diagonal elements of this equation gives Eq.3 below. However the non-diagonal part yields, $q = 0$ (see SI). Here we used $\beta_2 \approx \eta$ [10] and $\zeta \Delta\mu/\chi \simeq 1$.

$$\frac{1}{r} \partial_r (r \partial_r) \tilde{Q} - \left(\frac{1}{L_c^2} + \frac{4}{r^2} \right) \tilde{Q} = -\frac{\beta_1}{2L_c^2} \frac{\eta}{\zeta \Delta\mu} \left(\partial_r v_r - \frac{v_r}{r} \right) \quad (3)$$

Substitution of $H_{\alpha\beta} = -\beta_1 \beta_2 v_{\alpha\beta}$ into Eq.1 simply renormalizes the viscosity to $\tilde{\eta} = \eta(1 + \frac{1}{2}\beta_1^2)$. The resulting velocity equation (in polar form) using force balance yields

$$4\tilde{\eta} \partial_r \left(\partial_r + \frac{1}{r} \right) v_r = -\zeta \Delta\mu \left(\partial_r + \frac{2}{r} \right) \tilde{Q}, \quad (4)$$

Using zero influx $v_r(r_0) = 0$ at the outer boundary, and a stress free inner boundary $\sigma_{rr}(R_0) = 2\eta \partial_r v_r + \frac{\zeta \Delta\mu}{6} + \zeta \Delta\mu \tilde{Q} = 0$, we solve these two coupled equations numerically (using Mathematica), for different values of the flow coupling strength β_1 . The solutions are shown in Fig.1, using L_c as unit of length and $\frac{\eta}{\zeta \Delta\mu}$ as unit of time. It shows damping of the velocity field v_r with increase in flow coupling strength β_1 . Therefore, stronger flow coupling delays the ring closure time, however the order parameter profile, shown in the inset of Fig.1, appears to be almost unaffected by flow coupling strength β_1 . Note that, in this moving boundary problem, the major role

of the flow coupling on the OP is to move the boundary inward where the actin field gets realigned quickly. By setting $\tilde{Q}(R_0) = -1/2$ we have already captured this effect indirectly. This important observation allows us to ignore flow coupling in the OP equation here (r.h.s. of Eq.3) which can now be solved exactly. The general solution is $\tilde{Q}(r) = c_1 K_2(r/L_c) + c_2 I_2(r/L_c)$, where K_2 and I_2 are modified Bessel functions (see SI). For outer boundary $r_0 \rightarrow \infty$, we get

$$\tilde{Q}(r) = -K_2(r/L_c)/2K_2(R_0/L_c) \quad (5)$$

The solution for finite r_0 is given in the SI. The sharp rise in the magnitude of \tilde{Q} (irrespective of β_1) at the inner edge can be interpreted as the acto-myosin ring, of width L_c . Using this solution we can now solve for v_r (Eq.4) with arbitrary β_1 . For $r_0 \rightarrow \infty$, the solution reads,

$$\frac{v_r(r)}{\zeta\Delta\mu/\tilde{\eta}} = - \left[\left(1 + \frac{3K_1'(R_0/L_c)}{4K_2(R_0/L_c)} \right) \frac{R_0^2}{6r} + \frac{L_c}{8} \frac{K_1(r/L_c)}{K_2(R_0/L_c)} \right] \quad (6)$$

Note that the velocity at $r = R_0$, is the ring closure rate $v_r(R_0) = -\frac{\zeta\Delta\mu}{\tilde{\eta}} \frac{R_0}{6} \left[1 - \frac{3}{4} K_0(R_0/L_c)/K_2(R_0/L_c) \right]$, which is directly damped by the flow coupling strength β_1 via the effective viscosity $\tilde{\eta}$. Inclusion of cytoplasmic

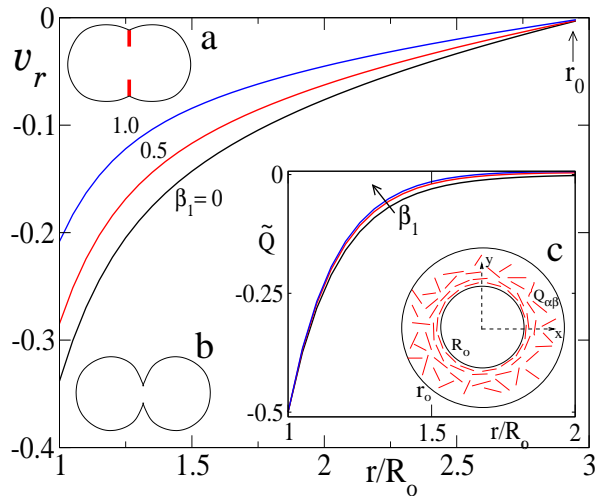


Figure 1: Solutions for the radially symmetric velocity field $v_r(r)$ (main figure) and the OP field $\tilde{Q}(r)$ (inset) are shown as a function of r/R_0 , for $R_0 = 5\mu\text{m}$. Schematic diagram 'a' shows sideview of the growing interface at the middle of the cell and 'c' shows its cross-sectional view ('b' shows partitioning without an interface). Alignment of filaments increases sharply near the inner boundary of the annulus at R_0 . The outer boundary is fixed at $r_0 = 15\mu\text{m}$ for these plots.

friction (αv_r), the velocity influx $v_r(r_0)$ at a finite outer boundary $r = r_0 > R_0$ (instead of $r_0 \rightarrow \infty$) can also influence the flow and the closure speed. Solutions for the boundary conditions $\tilde{Q}(r_0) = 0$ and $v_r(r_0) = 0$ are given in the SI.

Cytoplasmic friction adds αv_r to the right hand side of Eq.4 but does not alter the equation for \tilde{Q} . Restricting

ourselves to radial motion only (v_r nonzero, $v_\theta = 0$) and assuming azimuthal symmetry, we get

$$\left[\partial_r \left(\partial_r + \frac{1}{r} \right) - \frac{\alpha}{4\tilde{\eta}} \right] v_r = -\frac{\zeta\Delta\mu}{4\tilde{\eta}} \left(\partial_r + \frac{2}{r} \right) \tilde{Q}. \quad (7)$$

With boundary conditions $\tilde{Q}(r_0) = v_r(r_0) = 0$, and those at $r = R_0$ remaining same as before, we solve Eq.7, both using Green's function (see SI) and numerically in Mathematica. As expected, see Fig.2, cytoplasmic friction damps the flow at the growing interface and slows down the ring closure speed (inset of Fig.2).

The above analysis is carried out quasi-statically for a fixed R_0 . We can use these results to obtain the ring closure kinetics. We integrate the kinematic boundary condition $\frac{d}{dt}R_0 = v_r(R_0)$ to derive the time dependence of the radius of the contracting ring i.e., R_0 versus t . In Fig.2-inset we compare this closure rate with experimental data on *C. elegans* embryo [7, 22]. Note that this is a three parameter fit with α, β_1 and the active time scale $\frac{\eta}{\zeta\Delta\mu}$. Reasonable fits can be obtained for several combinations of these parameters in the range $\alpha, \beta_1 \in [0.1, 0.5]$ and $\frac{\eta}{\zeta\Delta\mu} \in [1.5, 2.5]\text{sec}$. One such example is shown in Fig.2-inset. Here we used $L_c = 1\mu\text{m}$ [22]. Membrane tension σ_0 in the growing membrane can be linked to the activity as $\sigma_0 = \zeta\Delta\mu e/2$ [10]. Using $\frac{\eta}{\zeta\Delta\mu} \simeq 2$ secs, measured value of cortical tension $\sigma_0 = 3 \times 10^{-4} \text{N/m}$ [23] and the thickness of the growing actomyosin cortex $e \simeq 0.3\mu\text{m}$ [22], we get $\eta \simeq 4 \times 10^3 \text{Pa}\cdot\text{sec}$, which is similar

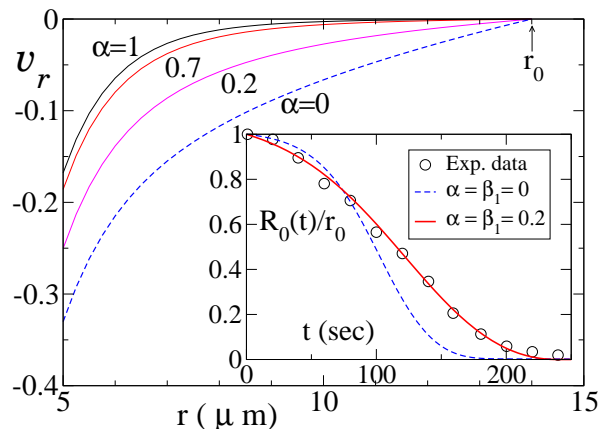


Figure 2: Cytoplasmic friction slows down the flow: v_r versus r in the main plot for different friction coefficients α . Inset: lines show scaled radius of the ring $R_0(t)/r_0$ versus time (sec), for $\alpha, \beta_1 = 0$ and nonzero values (see legends), with $\frac{\eta}{\zeta\Delta\mu} = 2.06\text{secs}$ for both. Furthermore, $r_0 = 14\mu\text{m}$, and $v_r(r_0) = 0$. Circles are the experimental data on *C. elegans* embryo [7, 22].

The ring closure rate in eukaryotes shows an intriguing slow down at late times (Fig2-inset), which has not been understood yet. In Ref [8] an adhoc intrinsic dynamic friction ζ_L was added, to the ring tension to account for

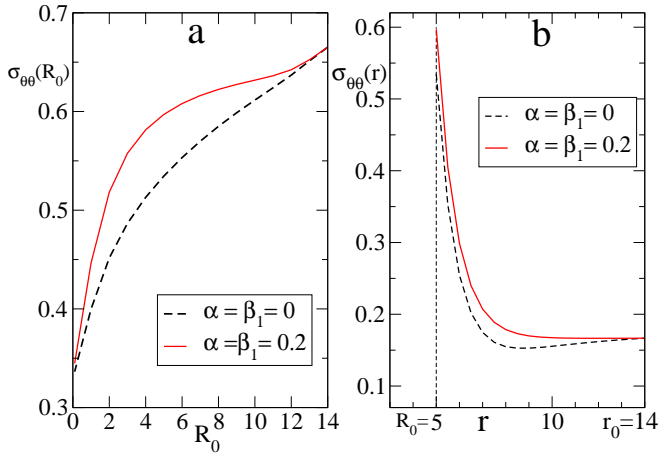


Figure 3: The line tension, (Eq.8), at the ring $\Sigma = \sigma_{\theta\theta}(R_0)$, in units of activity $\zeta\Delta\mu$, shown as a function of ring radius R_0 (in a), and as a function of r (in b), at a fixed $R_0 = 5\mu m$. The outer radius is fixed at $r_0 = 14\mu m$, appropriate for *C. elegans* embryo [7, 22]. Friction (nonzero α) does not affect ring tension significantly.

hitherto unknown internal processes in the ring. In Ref [4] the cortical flow from the poles, converging towards the equatorial furrow ($v_r(r_0)$ in our theory), was shown to affect the slow down [4]. In our present theory $\sigma_{\theta\theta}(r = R_0)$ is the effective ring tension Σ of Ref [8]. From Eq.1,

$$\sigma_{\theta\theta} = 2\eta \frac{v_r}{r} + \frac{\zeta\Delta\mu}{6} - \zeta\Delta\mu\tilde{Q}. \quad (8)$$

In Fig.3a we show the ring tension as a function of the ring size R_0 , and Fig.3b shows how azimuthal stress varies in the bulk of the closing interface, for a given ring size R_0 . First, $\sigma_{\theta\theta}$ is always positive, implying contractile stress in the ring and the interface. Second, the ring tension falls sharply at small R_0 , which explains the slow down. Third, the azimuthal stress $\sigma_{\theta\theta}(r)$ is very high at the edge $r = R_0$ and small in the interior. This property perfectly justifies the role of the ring as the main generator of cytokinetic tension. Note, that in Eq.8 the last two terms on the right hand side are constants (at the ring $r = R_0$), and positive. But the first term is negative and its magnitude grows large as the hole shrinks, eventually reducing the line tension. So the slowing down effect appears naturally due to viscosity of the flowing gel and curvature of the ring. Interestingly this tension reduction term has the same structure $v_r(R_0)/R_0 = \dot{R}_0/R_0$ which was assumed in Ref [8], based purely on phenomenology.

Stability of ring closure : We now use the rotationally symmetric solutions for the Q_{ij} and the \mathbf{v} fields to examine the stability of the inner boundary where the ring forms. This is motivated by the observation that wild type rings, during constriction, typically show deviation from circular shape [9, 22, 25], however it becomes more circular as constriction proceeds. Towards this we express the shape of the deformed inner boundary, at

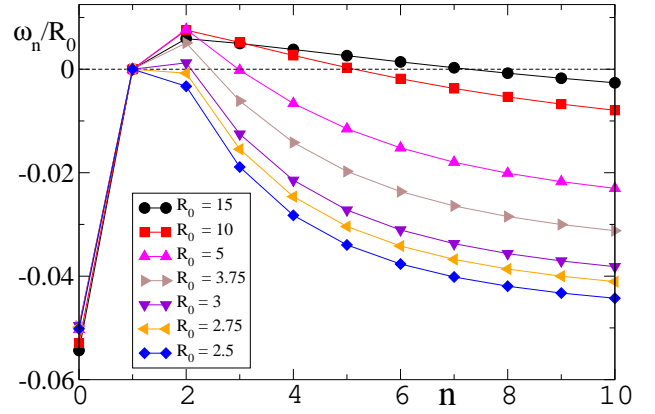


Figure 4: ω_n , scaled by the inner radius R_0 , as a function of the mode number n for different values of R_0 (μm), see legends. Low wave number modes switches from unstable to stable at smaller R_0 .

any given time, as $r(\theta) = R_0 + \delta R(\theta)$, and using Fourier decomposition $\delta R(\theta, t) = \sum_{n=0}^{\infty} \delta R_n e^{in\theta + \omega_n t}$. We study stability of these deformation modes [26] by computing ω_n , up to $n = 10$. Note that the $n = 1$ mode corresponds to an uniform translation of the inner circular boundary and therefore $\omega_1 = 0$. The system has translational symmetry provided the outer boundary $r_0 \rightarrow \infty$, which we exploit for this calculation. The results below are unlikely to change qualitatively when r_0 is finite, except that ω_1 will be nonzero.

The change at the inner edge leads to change in all the dynamical variables : $\tilde{Q}(r, \theta, t) = \tilde{Q}_0(r) + \delta\tilde{Q}(r, \theta, t)$, and similarly, $q(r, \theta, t) = \delta q(r, \theta, t)$, $v_r(r, \theta, t) = v_r^0(r) + \delta v_r(r, \theta, t)$, and $v_\theta(r, \theta, t) = \delta v_\theta(r, \theta, t)$.

Further, the perturbation fields $\delta\tilde{Q}, \delta q, \delta v_r$, and δv_θ can be decomposed into Fourier modes as $\delta\tilde{Q}(r, \theta, t) = \sum_{n=0}^{\infty} \delta\tilde{Q}_n(r) e^{in\theta + \omega_n t}$, $\delta v_r(r, \theta, t) = \sum_{n=0}^{\infty} \delta v_{r,n}(r) e^{in\theta + \omega_n t}$, and similarly for the other two fields.

We substitute these perturbed fields in the dynamical equations and do a linear stability analysis to obtain $\{\omega_n\}$, where $\omega_n = \partial_r v_r^0(R_0) + \frac{\delta v_{r,n}(R_0)}{\delta R_n}$, following Ref [26]. Details of our calculations are given in the SI.

Fig.4 reveals interesting behaviour for the growth rates of the Fourier modes $\{\omega_n\}$ for different inner radius R_0 . At large R_0 several modes are unstable ($\omega_n > 0$), however they subsequently turn stable ($\omega_n < 0$) as R_0 becomes small, absolutely consistent with experimental observations. Note that $\omega_0 < 0$, irrespective of R_0 , implies stability with respect to uniform contraction or expansion of the circular inner boundary. While in our theory ω_n is exactly proportional to the activity, Fig.4 shows that ω_0 is approximately proportional to R_0 . Also note that the higher modes decay relatively faster which would make any sharp distortion of the ring heal fast. This could be relevant for wound healing in cells as well. But the fact that larger number of modes are unstable at larger ring

size indicates that very large rings, if distorted, will fail to contract.

In summary, our phenomenological approximation on the boundary driven actomyosin alignment, was useful in obtaining exact solutions for the OP and the velocity field. The stability calculation, which produced several insights, exploited these solutions to perturb around them. Also we could identify three separate sources of slow down near the end of the constrictions, namely, a) the curvature at the ring ($1/R_0$), b) the cytoplasmic friction (α), and c) the flow coupling strength (β_1). Experiments along the lines of Ref[14] which probed poly/depolymerization processes near the ring and Ref[9] which studied healing of the perturbed ring after laser ablation, might be useful to assess the role of boundary in maintaining actin alignment in the dynamic ring.

Acknowledgement: We thank one of the referees for pointing out Ref[16] to us. MC would like to thank IIT Bombay, India for financial support. AN and AS acknowledge Science and Engineering Research Board (SERB), India Project No. ECR/2016/001967 and CRG/2019/005944, respectively, for financial support. MC and AC would like to thank Dr. R. Alert for sharing his stability calculations in Ref [26].

¹ Present address: Physics Department, MIT, Cambridge MA 02139, USA.

² asain@phy.iitb.ac.in, The 1st and the 2nd authors have contributed equally to this work.

[1] R. Rappaport, *Cytokinesis in animal cells* (Cambridge University Press, 1996).
 [2] R. A. Green, E. Paluch, and K. Oegema, Annual review of cell and developmental biology **28**, 29 (2012).
 [3] C. Guillot and T. Lecuit, Developmental cell **24**, 227 (2013).
 [4] H. Turlier, B. Audoly, J. Prost, and J.-F. Joanny, Biophysical journal **106**, 114 (2014).
 [5] D. Bray and J. White, Science **239**, 883 (1988).
 [6] J.-H. Zang and J. A. Spudich, Proceedings of the National Academy of Sciences **95**, 13652 (1998).
 [7] A. Zumdieck, K. Kruse, H. Bringmann, A. A. Hyman,

and F. Jülicher, PLoS one **2** (2007).
 [8] A. Sain, M. M. Inamdar, and F. Jülicher, Physical review letters **114**, 048102 (2015).
 [9] A. M. Silva, D. S. Osório, A. J. Pereira, H. Maiato, I. M. Pinto, B. Rubinstein, R. Gassmann, I. A. Telley, and A. X. Carvalho, J Cell Biol **215**, 789 (2016).
 [10] G. Salbreux, J. Prost, and J.-F. Joanny, Physical review letters **103**, 058102 (2009).
 [11] C. A. Mandato and W. M. Bement, The Journal of cell biology **154**, 785 (2001).
 [12] A.-C. Reymann, F. Staniscia, A. Erzberger, G. Salbreux, and S. W. Grill, Elife **5**, e17807 (2016).
 [13] F. Spira, S. Cuylen-Haering, S. Mehta, M. Samwer, A. Reversat, A. Verma, R. Oldenbourg, M. Sixt, and D. W. Gerlich, Elife **6**, e30867 (2017).
 [14] Y. Li and E. Munro, bioRxiv (2020).
 [15] J. Leite, F.-Y. Chan, D. S. Osório, J. Saramago, A. F. Sobral, A. M. Silva, R. Gassmann, and A. X. Carvalho, Frontiers in cell and developmental biology **8** (2020).
 [16] T. Chen, A. Callan-Jones, E. Fedorov, A. Ravasio, A. Brugués, H. T. Ong, Y. Toyama, B. C. Low, X. Trepát, T. Shemesh, et al., Nature physics **15**, 393 (2019).
 [17] P.-G. De Gennes and J. Prost, *The physics of liquid crystals*, vol. 83 (Oxford university press, 1993).
 [18] A. Carvalho, A. Desai, and K. Oegema, Cell **137**, 926 (2009).
 [19] K. Kruse, J.-F. Joanny, F. Jülicher, J. Prost, and K. Sekimoto, The European Physical Journal E **16**, 5 (2005).
 [20] M. C. Marchetti, J.-F. Joanny, S. Ramaswamy, T. B. Liverpool, J. Prost, M. Rao, and R. A. Simha, Reviews of Modern Physics **85**, 1143 (2013).
 [21] J. Prost, F. Jülicher, and J.-F. Joanny, Nature physics **11**, 111 (2015).
 [22] A. S. Maddox, L. Lewellyn, A. Desai, and K. Oegema, Developmental cell **12**, 827 (2007).
 [23] O. Thoumine, O. Cardoso, and J.-J. Meister, European Biophysics Journal **28**, 222 (1999).
 [24] F. Wottawah, S. Schinkinger, B. Lincoln, R. Ananthkrishnan, M. Romeyke, J. Guck, and J. Käs, Physical review letters **94**, 098103 (2005).
 [25] V. V. Menon, S. Soumya, A. Agarwal, S. R. Naganathan, M. M. Inamdar, and A. Sain, Biophysical journal **113**, 2787 (2017).
 [26] C. Pérez-González, R. Alert, C. Blanch-Mercader, M. Gómez-González, T. Kolodziej, E. Bazellieres, J. Casademunt, and X. Trepát, Nature Physics **15**, 79 (2019).

Supplementary Information : Part-I

Dynamics and stability of the contractile actomyosin ring in the cell

Mainak Chatterjee, Arkya Chatterjee, Amitabha Nandi, and Anirban Sain
Department of Physics, Indian Institute of Technology Bombay, Powai, Mumbai 400076, India

PACS numbers:

1. STRUCTURE OF THE ORDER PARAMETER MATRIX $Q_{\alpha\beta} = n_\alpha n_\beta - \delta_{\alpha\beta}/3$

1.1. $Q_{\alpha\beta}$ for filaments lying in the $x - y$ plane

When the filaments lie entirely in the $x - y$ plane, i.e., $\hat{n} = (n_x, n_y, 0)$ then the symmetric, traceless matrix,

$$\mathbb{Q} = \begin{bmatrix} Q_1 & q & 0 \\ q & Q_2 & 0 \\ 0 & 0 & -1/3 \end{bmatrix}, \text{ with } Q_1 + Q_2 = 1/3$$

When the distribution of filaments is random (isotropic) in the X-Y plane then due to $\langle n_x^2 \rangle = \langle n_y^2 \rangle = 1/2$ and $n_z = 0$, the resulting \mathbb{Q}^0 is diagonal, with $Q_{xx} = Q_{yy} = 1/6$ and $Q_{zz} = -1/3$. Due to flow or boundary condition \mathbb{Q} will deviate from its isotropic form and thus, $\mathbb{Q} = \mathbb{Q}^0 + \mathbb{Q}'$. Explicitly,

$$\begin{bmatrix} Q_1 & q & 0 \\ q & Q_2 & 0 \\ 0 & 0 & -1/3 \end{bmatrix} = \begin{bmatrix} 1/6 & 0 & 0 \\ 0 & 1/6 & 0 \\ 0 & 0 & -1/3 \end{bmatrix} + \begin{bmatrix} q_1 & q & 0 \\ q & q_2 & 0 \\ 0 & 0 & 0 \end{bmatrix}, \text{ preserving symmetric structure of the L.H.S. .}$$

Further, \mathbb{Q}' also must be traceless, since \mathbb{Q} and \mathbb{Q}^0 are already traceless, and thus $q_1 = -q_2$ ($= \tilde{Q}$ in the main text).

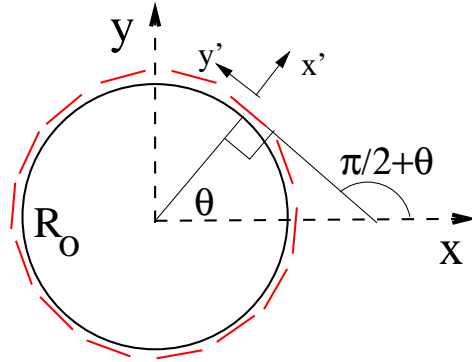


Figure 1: Nematic aligned along the azimuthal direction

1.2. Boundary condition for the order parameter $Q_{\alpha\beta}$

We impose that the acto-myosin filaments (red lines in Fig.1 below) be completely aligned with the circular inner boundary, at $r = R_0$, i.e., they are parallel to the azimuthal direction $\hat{\theta}$. At the outer boundary, either at a finite radius $r_0 > R_0$) or at $r \rightarrow \infty$, the filaments are randomly oriented. This is a phenomenological input to our theory, ensuring that an acto-myosin ring forms at the open edge of the inward growing membrane. Below, we derive the corresponding order parameter tensor in the cylindrical polar coordinates.

Let the nematic director on the ring, at an angle θ , be oriented along $\hat{n}(\theta)$, (see Fig.1). In the Cartesian reference frame (x, y) , $\hat{n}(\theta) = (n_x, n_y, 0) = \hat{\theta} = (-\sin \theta, \cos \theta, 0)$. The resulting order parameter matrix at $r = R_0$ is then

$$\mathbb{Q}(R_0, \theta) = \begin{bmatrix} n_x^2 - \frac{1}{3} & n_x n_y & 0 \\ n_x n_y & n_y^2 - \frac{1}{3} & 0 \\ 0 & 0 & -1/3 \end{bmatrix} = \begin{bmatrix} \sin^2 \theta - \frac{1}{3} & -\frac{\sin 2\theta}{2} & 0 \\ -\frac{\sin 2\theta}{2} & \cos^2 \theta - \frac{1}{3} & 0 \\ 0 & 0 & -\frac{1}{3} \end{bmatrix}$$

But \mathbb{Q} has a simple form in the polar coordinate frame $(\hat{r}, \hat{\theta})$, which is obtained from the original cartesian frame (x, y) via a counter-clockwise rotation (by angle θ). In the polar frame, $\hat{n}(\theta) = (0, 1, 0)$, and thus,

$$\mathbb{Q}^p(R_0, \theta) = \begin{bmatrix} -1/3 & 0 & 0 \\ 0 & 2/3 & 0 \\ 0 & 0 & -1/3 \end{bmatrix}.$$

Here the superscript p denotes polar. We seek the same decomposition of \mathbb{Q}^p into isotropic and deviation parts: $\mathbb{Q}^p = \mathbb{Q}^{0p} + \mathbb{Q}'^p$. However \mathbb{Q}^{0p} remains same in the two coordinate frames. Thus,

$$\mathbb{Q}'^p(R_0, \theta) = \begin{bmatrix} -1/3 & 0 & 0 \\ 0 & 2/3 & 0 \\ 0 & 0 & -1/3 \end{bmatrix} - \begin{bmatrix} 1/6 & 0 & 0 \\ 0 & 1/6 & 0 \\ 0 & 0 & -1/3 \end{bmatrix} = \begin{bmatrix} -1/2 & 0 & 0 \\ 0 & 1/2 & 0 \\ 0 & 0 & 0 \end{bmatrix}. \quad (1)$$

This serves as the boundary condition at $r = R_0$ in our radially symmetric formulation. Here we obtained the polar forms of the \mathbb{Q} matrices using the transformed form of director \hat{n} in the polar frame. One could also transform the \mathbb{Q} matrix from the cartesian frame (x, y) to the polar frame $(\hat{r}, \hat{\theta})$, using $\mathbb{Q}^p = R\mathbb{Q}R^{-1}$, where R is the rotation matrix for counter-clockwise passive rotation about \hat{z} axis, by angle θ . More explicitly,

$$\mathbb{Q}^p = \begin{bmatrix} \cos \theta & \sin \theta & 0 \\ -\sin \theta & \cos \theta & 0 \\ 0 & 0 & 1 \end{bmatrix} \begin{bmatrix} \sin^2 \theta - \frac{1}{3} & -\frac{\sin 2\theta}{2} & 0 \\ -\frac{\sin 2\theta}{2} & \cos^2 \theta - \frac{1}{3} & 0 \\ 0 & 0 & -\frac{1}{3} \end{bmatrix} \begin{bmatrix} \cos \theta & -\sin \theta & 0 \\ \sin \theta & \cos \theta & 0 \\ 0 & 0 & 1 \end{bmatrix} = \begin{bmatrix} -1/3 & 0 & 0 \\ 0 & 2/3 & 0 \\ 0 & 0 & -1/3 \end{bmatrix} \quad (2)$$

Using the same transformation on \mathbb{Q}^0 one can show that the isotropic part remain unchanged in the polar frame.

2. CONSTITUTIVE RELATIONS AND THE FORCE-BALANCE EQUATION IN 2D POLAR COORDINATES

Recall the constitutive equations (Eq. (2),(3) in the maintext) for the stress and the nematic order parameter

$$\sigma_{\alpha\beta} = 2\eta v_{\alpha\beta} - \beta_1 H_{\alpha\beta} + \zeta \Delta\mu Q_{\alpha\beta}, \quad (3)$$

$$\frac{D}{Dt} Q_{\alpha\beta} = \beta_1 v_{\alpha\beta} + \frac{1}{\beta_2} H_{\alpha\beta}. \quad (4)$$

In the steady state $H_{\alpha\beta} = -\beta_1 \beta_2 v_{\alpha\beta}$. Substitution of $H_{\alpha\beta}$ into Eq.3 renormalises the viscosity to $\bar{\eta} = \eta(1 + \frac{\beta_1^2 \beta_2}{2\eta})$. Further, using the definition $Q_{\alpha\beta} = Q_{\alpha\beta}^0 + Q'_{\alpha\beta}$ and retaining the same notation η (henceforth) for the renormalised viscosity, the components of the stress tensor given in Eq. 3 can be written in 2D polar coordinates (r, θ) as:

$$\sigma_{rr} = 2\eta \partial_r v_r + \frac{\zeta \Delta\mu}{6} + \zeta \Delta\mu \tilde{Q}, \quad (5)$$

$$\sigma_{r\theta} = \eta \left(\frac{1}{r} \partial_\theta v_r + \partial_r v_\theta - \frac{v_\theta}{r} \right) + \zeta \Delta\mu q, \quad (6)$$

$$\sigma_{\theta r} = \sigma_{r\theta}, \quad (7)$$

$$\sigma_{\theta\theta} = 2\frac{\eta}{r} (\partial_\theta v_\theta + v_r) + \frac{\zeta \Delta\mu}{6} - \zeta \Delta\mu \tilde{Q}. \quad (8)$$

Here $\sigma_{rz} = \sigma_{zr} = \sigma_{\theta z} = \sigma_{z\theta} = 0$. The components of the strain rate tensor $v_{\alpha\beta}$, in polar coordinates, are

$$v_{\alpha\beta} = \begin{bmatrix} \partial_r v_r & \frac{1}{2} \left\{ \frac{1}{r} \partial_\theta v_r + r \partial_r \left(\frac{v_\theta}{r} \right) \right\} \\ \frac{1}{2} \left\{ \frac{1}{r} \partial_\theta v_r + r \partial_r \left(\frac{v_\theta}{r} \right) \right\} & \frac{1}{r} (v_r + \partial_\theta v_\theta) \end{bmatrix} \quad (9)$$

Furthermore we obtain σ_{zz} using the traceless condition.

$$\sigma_{zz} = -(\sigma_{rr} + \sigma_{\theta\theta}) = -2\eta \left(\frac{1}{r}v_r + \partial_r v_r + \frac{1}{r}\partial_\theta v_\theta \right) - \frac{\zeta\Delta\mu}{3} \quad (10)$$

Now we define the effective 2D tension tensor for the cortical layer $t_{ij} = \int dz(\sigma_{ij} - P\delta_{ij})$ [1]. As explained in maintext (originally from Ref[1]), $P = \sigma_{zz}$. The corresponding force balance equations, $\partial_j t_{ij} = \alpha v_i$, in polar coordinates read

$$\partial_r t_{rr} + \frac{1}{r}(t_{rr} - t_{\theta\theta}) + \frac{1}{r}\partial_\theta t_{r\theta} = \alpha v_r, \quad (11)$$

$$\partial_r t_{\theta r} + \frac{1}{r}(t_{\theta r} + t_{r\theta}) + \frac{1}{r}\partial_\theta t_{\theta\theta} = \alpha v_\theta. \quad (12)$$

Substituting Eqs. (5–10) and Eq.6 from maintext into Eqs. (11–12), we get the full expression of the force-balance equation

$$2\eta \left(2\frac{\partial}{\partial r} \left(\frac{\partial}{\partial r} + \frac{1}{r} \right) v_r + \frac{3}{2}\frac{\partial}{\partial r} \left(\frac{\partial}{\partial \theta} \frac{v_\theta}{r} \right) + \frac{\partial}{\partial \theta} \left(\frac{\partial}{\partial \theta} \frac{v_r}{2r^2} \right) - \frac{\partial}{\partial \theta} \frac{v_\theta}{r^2} \right) + \zeta\Delta\mu \left(\left(\frac{\partial}{\partial r} + \frac{2}{r} \right) \tilde{Q} + \frac{\partial}{\partial \theta} \frac{q}{r} \right) = \alpha v_r, \quad (13)$$

$$\eta \left(\frac{\partial}{\partial r} \left(\frac{\partial}{\partial r} v_\theta \right) + 3\frac{\partial}{\partial r} \left(\frac{\partial}{\partial \theta} \frac{v_r}{r} \right) + 5\frac{\partial}{\partial \theta} \frac{v_r}{r^2} + 4\frac{\partial}{\partial \theta} \left(\frac{\partial}{\partial \theta} \frac{v_\theta}{r^2} \right) - \frac{v_\theta}{r^2} + \frac{1}{r}\frac{\partial}{\partial r} v_\theta \right) + \zeta\Delta\mu \left(\left(\frac{\partial}{\partial r} + \frac{2}{r} \right) q - \frac{\partial}{\partial \theta} \frac{\tilde{Q}}{r} \right) = \alpha v_\theta. \quad (14)$$

These equations are formidable to solve. We look for solutions with azimuthal symmetry and also assume $v_\theta = 0$. In the main text we had obtained solutions for $v_r(r)$ and $\tilde{Q}(r)$ by numerically solving Eq.3,4 (one can show $q = 0$, see below). We showed that, in steady-state ($\frac{D}{Dt}Q_{\alpha\beta} = 0$), with the boundary condition that the nematics are perfectly aligned with the inner perimeter ($r = R_0$), the solutions for \tilde{Q} are very weakly dependent on β_1 , the flow coupling parameter. However, $v_r(r)$ strongly depends on β_1 , via viscosity renormalisation. Therefore we simplify Eq.4 by setting $\beta_1 = 0$ and get $H_{\alpha\beta} = 0$. Further using Landau-De Gennes energy functional (mentioned in the maintext), for $H_{\alpha\beta}$ we get,

$$\nabla^2 \tilde{Q} = \frac{\tilde{Q}}{L_c^2}, \quad \nabla^2 q = \frac{q}{L_c^2}, \quad (15)$$

Here $L_c = \sqrt{L/\chi}$ is the nematic correlation length scale. Converting Eq. 15 into polar form we get (derivation given in section-4)

$$\frac{1}{r}\frac{\partial}{\partial r} \left(r\frac{\partial \tilde{Q}}{\partial r} \right) - \left(\frac{1}{L_c^2} + \frac{4}{r^2} \right) \tilde{Q} = 0 \quad (16)$$

$$\frac{1}{r}\frac{\partial}{\partial r} \left(r\frac{\partial q}{\partial r} \right) - \left(\frac{1}{L_c^2} + \frac{4}{r^2} \right) q = 0 \quad (17)$$

The force-balance equations, Eqs. (13–14), further simplifies to:

$$4\eta\frac{\partial}{\partial r} \left(\frac{\partial}{\partial r} + \frac{1}{r} \right) v_r + \zeta\Delta\mu \left(\frac{\partial}{\partial r} + \frac{2}{r} \right) \tilde{Q} = \alpha v_r \quad (18)$$

$$\frac{\partial q}{\partial r} + \frac{2q}{r} = 0 \quad (19)$$

Eqs. (16–17) and Eqs. (18–19) are the main equations used in our study for $\beta_1 = 0$. We now look at several limiting cases using these set of equations.

2.1. Nematic order with $\beta_1 = 0$.

Substituting Eq. 19 in Eq. 17, we get $q = 0$. Furthermore we notice that Eq. 16 is a modified Bessel equation of order 2 [2]. This has solution of the form

$$\tilde{Q}(r) = c_1 K_2(r/L_c) + c_2 I_2(r/L_c), \quad (20)$$

where I_2 and K_2 are the modified Bessel functions of the second kind [2]. Since I_2 blows up as $r \rightarrow \infty$, we set $c_2 = 0$. Using the other boundary condition i.e., $\tilde{Q}(r = R_0) = -\frac{1}{2}$ (see Sec.), we get $c_1 = -\frac{1}{2K_2(R_0/L_c)}$. The zeroth-order solution for the nematic order parameter is then given by

$$\tilde{Q}^0(r) = -\frac{K_2(r/L_c)}{2K_2(R_0/L_c)}, \quad (21)$$

which is Eq. 5 in the main-text.

Instead of having the outer boundary at infinity, if it is located at $r = r_0 > R_0$ (which is the realistic case since at the division plane the cell has a finite cross-section), then using $\tilde{Q} = 0$ at $r = r_0$ (keeping the other boundary condition at R_0 unchanged), we get

$$\tilde{Q}^0(r) = -\frac{I_2(r)K_2(r_0) - K_2(r)I_2(r_0)}{2[I_2(R_0)K_2(r_0) - K_2(R_0)I_2(r_0)]}, \quad (22)$$

2.2. Flow field in the absence of substrate friction

In the absence of substrate friction (i.e., $\alpha = 0$), Eq. 18 becomes

$$\frac{\partial}{\partial r} \left(\frac{\partial}{\partial r} + \frac{1}{r} \right) v_r + \frac{\zeta \Delta \mu}{4\eta} \left(\frac{\partial}{\partial r} + \frac{2}{r} \right) \tilde{Q} = 0. \quad (23)$$

Substituting Eq. 21 in Eq. 23, we get a second order differential equation in v_r with a source term, namely,

$$\frac{\partial}{\partial r} \left(\frac{\partial}{\partial r} + \frac{1}{r} \right) v_r = -\frac{\zeta \Delta \mu}{4\eta} \frac{K_1(r/L_c)}{2K_2(R_0/L_c)}. \quad (24)$$

The homogeneous solution of Eq. 24 is of the form $(Ar + B/r)$. To obtain the particular solution, we use an ansatz $v_p(r) = \Omega K_1(r/L_c)$. This is inspired by the form of the source term in Eq. 24. Substituting this particular solution in Eq. 24 gives us $\Omega = -\frac{\zeta \Delta \mu}{4\eta} \frac{L_c}{2K_2(R_0/L_c)}$. The general solution for v_r is then given by

$$v_r(r) = Ar + \frac{B}{r} - \frac{\zeta \Delta \mu}{4\eta} \frac{L_c}{2K_2(R_0/L_c)} K_1(r/L_c). \quad (25)$$

We put $A = 0$, since $v_r \rightarrow 0$ as $r \rightarrow \infty$. The constant B is calculated using the free boundary condition at $r = R_0$, i.e. $\sigma_{rr}(R_0) = 0$. Using this condition in Eq. 5, we get a boundary condition for v'_r at R_0 , which is given by

$$2\eta v'_r(R_0) + \frac{\zeta \Delta \mu}{6} - \frac{\zeta \Delta \mu}{2} = 0. \quad (26)$$

Using Eq. 25 and Eq. 26 we get $B = -\frac{\zeta \Delta \mu R_0^2}{6\eta} \left[1 + \frac{K'_1(R_0/L_c)}{K_2(R_0/L_c)} \right]$, which leads to the final expression for the zeroth-order velocity field $v_r^0(r)$ (Eq. 6 in the maintext), namely,

$$v_r^0(r) = -\frac{\zeta \Delta \mu}{\eta} \left[\left(1 + \frac{3K'_1(R_0/L_c)}{4K_2(R_0/L_c)} \right) \frac{R_0^2}{6r} + \frac{L_c}{8} \frac{K_1(r/L_c)}{K_2(R_0/L_c)} \right] \quad (27)$$

The corresponding velocity equation, for the case of outer boundary located at finite $r = r_0$, and $v_r(r_0) = 0$ (keeping the other stress boundary condition at $r = R_0$ unchanged) is solved numerically using Mathematica.

2.3. Flow-field in the presence of substrate friction

Here we consider the rotationally symmetric case but in the presence of substrate friction ($\alpha \neq 0$). The force-balance equation given by Eq. 18 can be re-written as

$$\underbrace{\left[\partial_r \left(\partial_r + \frac{1}{r} \right) - \tilde{\alpha} \right]}_{\mathcal{L}} v_r = f(r). \quad (28)$$

Here $\tilde{\alpha} = \frac{\alpha}{4\eta}$ and $f(r) = -\frac{\zeta\Delta\mu}{4\eta} \left(\partial_r + \frac{2}{r} \right) \tilde{Q}_0 = -\frac{\zeta\Delta\mu}{4\eta} \frac{K_1(r/L_c)}{2K_2(R_0/L_c)}$. Here $\tilde{Q}_0(r)$ is the zeroth-order solution obtained for $\beta_1 = 0$ (see Eq. 21). Eq. 28 is a linear non-homogenous differential equation and can be solved using the method of Green's function with boundary conditions $v_r(r \rightarrow \infty) = 0$, and $\sigma_{rr}(R_0) = 0$.

The Green's function $G(r, r')$ for the differential operator \mathcal{L} appearing in Eq. 28 satisfies the differential equation:

$$\mathcal{L}G(r, r') = \left[\frac{\partial^2}{\partial r^2} + \frac{1}{r} \frac{\partial}{\partial r} - \frac{1}{r^2} (\tilde{\alpha}r^2 + 1) \right] G(r, r') = \delta(r - r'). \quad (29)$$

Eq. 29 is a modified Bessel equation of first order. This general solution is written in terms of the modified Bessel functions of first and second kind.

$$r < r' \quad : \quad G(r, r') = G_{<}(r, r') = A_1 I_1(\sqrt{\tilde{\alpha}}r) + A_2 K_1(\sqrt{\tilde{\alpha}}r), \quad (30)$$

$$r > r' \quad : \quad G(r, r') = G_{>}(r, r') = B_1 I_1(\sqrt{\tilde{\alpha}}r) + B_2 K_1(\sqrt{\tilde{\alpha}}r). \quad (31)$$

The full solution to Eq. 28 can be written as,

$$v_r(r) = v_h(r) + \int_{R_0}^{\infty} G(r, r') f(r') dr'. \quad (32)$$

Here $v_h(r)$ represents the homogeneous solution obtained by solving $\mathcal{L}v_r = 0$. It is easy to check that it is given by

$$v_h(r) = -\frac{\zeta\Delta\mu}{3\eta\sqrt{\tilde{\alpha}}} \frac{K_1(\sqrt{\tilde{\alpha}}r)}{K_0(R_0\sqrt{\tilde{\alpha}}) + K_2(R_0\sqrt{\tilde{\alpha}})} \quad (33)$$

The unknown constants in Eqs. (30-31) are determined from the boundary conditions. Here $G(r, r')$ is defined in the range $[R_0, \infty)$. By using the known boundary conditions for v_r and substituting the expression of Eq. 33 in Eq. 32, we notice that $G(r, r')$ should satisfy the following boundary conditions at $r = R_0$ and $r \rightarrow \infty$ respectively

$$\partial_r G(r, r') \Big|_{r=R_0} = 0, \quad (34)$$

$$G(r \rightarrow \infty, r') = 0. \quad (35)$$

Eqs. (35,34) give $B_1 = 0$ and $A_1 = A_2 \frac{K_0(\sqrt{\tilde{\alpha}}R_0) + K_2(\sqrt{\tilde{\alpha}}R_0)}{I_0(\sqrt{\tilde{\alpha}}R_0) + I_2(\sqrt{\tilde{\alpha}}R_0)}$, respectively. The remaining two boundary conditions are obtained by integrating Eq. 29 twice over an infinitesimally small interval around r' . This gives the continuity conditions of $G(r, r')$ and its derivative at $r = r'$, namely,

$$\frac{\partial G_{>}}{\partial r} \Big|_{r \rightarrow r'_+} - \frac{\partial G_{<}}{\partial r} \Big|_{r \rightarrow r'_-} = 1, \quad (36)$$

$$G_{<}(r, r') \Big|_{r \rightarrow r'_-} = G_{>}(r, r') \Big|_{r \rightarrow r'_+}. \quad (37)$$

Eqs. (36,37) give $B_2 = \frac{A_2(K_0(\sqrt{\tilde{\alpha}}R_0) + K_2(\sqrt{\tilde{\alpha}}R_0))I_1(r'\sqrt{\tilde{\alpha}})}{(I_0(\sqrt{\tilde{\alpha}}R_0) + I_2(\sqrt{\tilde{\alpha}}R_0))K_1(r'\sqrt{\tilde{\alpha}})} + A_2$, where

$$A_2 = -\frac{2 \cdot (I_0(\sqrt{\tilde{\alpha}}R_0) + I_2(\sqrt{\tilde{\alpha}}R_0))}{\sqrt{\tilde{\alpha}}r' (K_0(\sqrt{\tilde{\alpha}}R_0) + K_2(\sqrt{\tilde{\alpha}}R_0)) (K_0(r'\sqrt{\tilde{\alpha}}) + K_2(r'\sqrt{\tilde{\alpha}})) \left(\frac{I_1(r'\sqrt{\tilde{\alpha}})}{K_1(r'\sqrt{\tilde{\alpha}})} + \frac{(I_0(r'\sqrt{\tilde{\alpha}}) + I_2(r'\sqrt{\tilde{\alpha}}))}{K_0(r'\sqrt{\tilde{\alpha}}) + K_2(r'\sqrt{\tilde{\alpha}})} \right)}$$

The full solution is now written as:

$$v_r(r) = -\frac{\zeta\Delta\mu}{3\eta\sqrt{\tilde{\alpha}}} \frac{K_1(\sqrt{\tilde{\alpha}}r)}{K_0(R_0\sqrt{\tilde{\alpha}}) + K_2(R_0\sqrt{\tilde{\alpha}})} + \int_{R_0}^r G_{>}(r, r') f(r') dr' + \int_r^{\infty} G_{<}(r, r') f(r') dr'. \quad (38)$$

The two integrals in Eq. 38 are evaluated numerically, for different values of r , using "NIntegrate" in Mathematica. The constants R_0, α are kept fixed. In this manner we obtain a table for v_r (in units of $\frac{\zeta\Delta\mu}{\eta}$) versus r .

3. CORRECTION TO THE NEMATIC FIELD DUE TO NON-ZERO β_1

We have already shown numerically (main-text) that the correction to $\tilde{Q}(r)$ is small even for finite β_1 . This correction can be estimated for small β_1 perturbatively, up to different orders in β_1 , using Greens function approach. For that we use the zeroth order solution v_r^0 (Eq.27 with bare viscosity η , corresponding to $\beta_1 = 0$), on the right hand side of Eq.3, in the main-text, which now reads,

$$\partial_r (r\partial_r) \tilde{Q} - \left(\frac{r}{L_c^2} + \frac{4}{r} \right) \tilde{Q} = -\frac{1}{2L} \beta_1 \beta_2 r \left(\partial_r v_r^0 - \frac{v_r^0}{r} \right). \quad (39)$$

Substituting for v_r^0 we get,

$$\partial_r (r\partial_r) \tilde{Q} - \frac{r}{L_c^2} \tilde{Q} - \frac{4}{r} \tilde{Q} = -\frac{\beta_1 \beta_2 r}{2L} \left(\frac{R_0^2 \left(5 - \frac{3K_0(R_0/L_c)}{K_2(R_0/L_c)} \right)}{24r^2} + \frac{\frac{L_c}{r} K_1(r/L_c) + \frac{1}{2}(K_0(r/L_c) + K_2(r/L_c))}{8K_2(R_0/L_c)} \right) \quad (40)$$

which can be re-written as follows

$$\underbrace{\left[\partial_r (r\partial_r) - \frac{r}{L_c^2} - \frac{4}{r} \right]}_{\mathcal{L}} \tilde{Q} = u(r), \quad (41)$$

where $u(r)$ is the right hand side of Eq.39. The boundary conditions on \tilde{Q} are: $\tilde{Q}(r \rightarrow \infty) = 0$, and $\tilde{Q}(r \rightarrow R_0) = -0.5$. The Green's function $G(r, r')$ for operator \mathcal{L} in Eq. 41 satisfies the modified Bessel equation of order 2.

$$\mathcal{L}G(r, r') = \left[\partial_r (r\partial_r) - \frac{r}{L_c^2} - \frac{4}{r} \right] G(r, r') = \delta(r - r'), \quad (42)$$

having a solution of the form

$$r < r' : \quad G(r, r') = G_<(r, r') = A_1 I_2(r) + A_2 K_2(r), \quad (43)$$

$$r > r' : \quad G(r, r') = G_>(r, r') = B_1 I_2(r) + B_2 K_2(r). \quad (44)$$

The four unknown constants can be determined from the boundary conditions on $G(r, r')$ which as before are given by,

$$G(r \rightarrow R_0, r') = 0, \quad (45)$$

$$G(r \rightarrow \infty, r') = 0, \quad (46)$$

$$\frac{\partial G_>}{\partial r} \Big|_{r \rightarrow r'_+} - \frac{\partial G_<}{\partial r} \Big|_{r \rightarrow r'_-} = 1, \quad (47)$$

$$G_<(r, r') \Big|_{r \rightarrow r'_-} = G_>(r, r') \Big|_{r \rightarrow r'_+}. \quad (48)$$

Eq. (45–48) gives $B_1 = 0$, $A_2 = -\frac{A_1 I_2(R_0)}{K_2(R_0)}$, $B_2 = A_1 \left(\frac{I_2(r')}{K_2(r')} - \frac{I_2(R_0)}{K_2(R_0)} \right)$, and $A_1 = \frac{K_2(r')}{r'(I_2(r')K_2'(r') - I_2'(r')K_2(r'))}$. The full solution to Eq. 41 is therefore

$$\tilde{Q}(r) = \tilde{Q}_h(r) + \int_{R_0}^{\infty} G(r, r') u(r') dr', \quad (49)$$

where $\tilde{Q}_h(r) = -\frac{K_2(r/L_c)}{2K_2(R_0/L_c)}$ is homogeneous solution obtained by solving $\mathcal{L}\tilde{Q} = 0$. The full solution can then be rewritten as:

$$\tilde{Q} = -\frac{K_2(r/L_c)}{2K_2(R_0/L_c)} + \int_{R_0}^r G_>(r, r') u(r') dr' + \int_r^{\infty} G_<(r, r') u(r') dr'. \quad (50)$$

The corresponding velocity equation (Eq.18) is easy to handle in the small β_1 limit. Substituting \tilde{Q}^0 in place of \tilde{Q} gives us

$$4\eta \partial_r \left(\partial_r + \frac{1}{r} \right) v_r = -\frac{\zeta \Delta \mu}{1 + \frac{\beta_1^2 \beta_2}{2\eta}} \left(\partial_r + \frac{2}{r} \right) \tilde{Q}_0 \quad (51)$$

Note that this equation has the same structure as Eq.23, with the viscosity η enhanced by a factor of $(1 + \frac{\beta_1^2 \beta_2}{2\eta})$. Therefore the solution is same as Eq.27, where η has to be replaced by $\eta(1 + \frac{\beta_1^2 \beta_2}{2\eta})$.

4. DERIVATION OF DYNAMICAL EQUATIONS FOR \tilde{Q}, q (EQ.16,17 FROM EQ.15)

The polar form of $Q'_{\alpha\beta}$ matrix, $\begin{bmatrix} Q'_{rr} & Q'_{r\theta} \\ Q'_{\theta r} & Q'_{\theta\theta} \end{bmatrix}$, is given by

$$\begin{bmatrix} \cos \theta & \sin \theta \\ -\sin \theta & \cos \theta \end{bmatrix} \begin{bmatrix} \tilde{Q} & q \\ q & -\tilde{Q} \end{bmatrix} \begin{bmatrix} \cos \theta & -\sin \theta \\ \sin \theta & \cos \theta \end{bmatrix} = \begin{bmatrix} \tilde{Q} \cos 2\theta + q \sin 2\theta & q \cos 2\theta - \tilde{Q} \sin 2\theta \\ q \cos 2\theta - \tilde{Q} \sin 2\theta & -(\tilde{Q} \cos 2\theta + q \sin 2\theta) \end{bmatrix} \equiv \begin{bmatrix} Q_1 & q_1 \\ q_1 & -Q_1 \end{bmatrix} \quad (52)$$

where $\begin{bmatrix} \tilde{Q} & q \\ q & -\tilde{Q} \end{bmatrix}$ is its corresponding cartesian form (in $x-y$). Noting that the basic structure of the matrix is retained, we express the new matrix elements in terms of the old ones as, $Q_1 = \tilde{Q} \cos 2\theta + q \sin 2\theta$ and, $q_1 = -\tilde{Q} \sin 2\theta + q \cos 2\theta$. Inverting these we get, $\tilde{Q} = Q_1 \cos 2\theta - q_1 \sin 2\theta$ and, $q = Q_1 \sin 2\theta + q_1 \cos 2\theta$. Note that Q_1, q_1 are functions of r via \tilde{Q}, q . Now substituting the polar form for the laplacian operator and \tilde{Q} into Eq.15, $\nabla^2 \tilde{Q} = \frac{\tilde{Q}}{L_c^2}$ (whose polar form we are interested in), we get

$$\begin{aligned} \left[\frac{1}{r} \frac{\partial}{\partial r} \left(r \frac{\partial}{\partial r} \right) + \frac{1}{r^2} \frac{\partial^2}{\partial \theta^2} \right] (Q_1 \cos 2\theta - q_1 \sin 2\theta) &= \frac{Q_1 \cos 2\theta - q_1 \sin 2\theta}{L_c^2} \\ \frac{1}{r} \frac{\partial}{\partial r} \left(r \frac{\partial Q_1}{\partial r} \right) \cos 2\theta - \frac{1}{r} \frac{\partial}{\partial r} \left(r \frac{\partial q_1}{\partial r} \right) \sin 2\theta - \frac{Q_1}{r^2} 4 \cos 2\theta + \frac{q_1}{r^2} 4 \sin 2\theta &= \frac{Q_1 \cos 2\theta - q_1 \sin 2\theta}{L_c^2} \end{aligned} \quad (53)$$

Further, separating the coefficients of $\cos 2\theta$ and $\sin 2\theta$ from the two sides, yields

$$\left[\frac{1}{r} \frac{\partial}{\partial r} \left(r \frac{\partial Q_1}{\partial r} \right) - 4 \frac{Q_1}{r^2} - \frac{Q_1}{L_c^2} \right] \cos 2\theta - \left[\frac{1}{r} \frac{\partial}{\partial r} \left(r \frac{\partial q_1}{\partial r} \right) - 4 \frac{q_1}{r^2} - \frac{q_1}{L_c^2} \right] \sin 2\theta = 0 \quad (54)$$

Since $\cos 2\theta$ and $\sin 2\theta$ are independent functions their coefficients, separately, must be zero. Thus we obtain the order parameter equations Eq.16 and Eq.17, where we retained the same notations as in the cartesian frame, by changing $(Q_1, q_1) \rightarrow (\tilde{Q}, q)$.

5. COMPUTATION OF CLOSURE RATE $R_0(t)$ VS t .

This requires the velocity at the ring $v_r(R_0)$ for different values of R_0 . When the outer radius is located at infinity we have a closed form expression for $v_r(R_0)$ which can be integrated to obtain the closure rate. But for the case of finite outer boundary (at r_0) we could solve the velocity equation (Eq.18) only numerically (using "NDSolve" in Mathematica) after incorporating the analytic expression for $\tilde{Q}^0(r)$ (Eq.22). Therefore we first prepared a table for $v_r(R_0)$ versus R_0 by solving the velocity equation for different values of R_0 . We then obtained an interpolation function for this table. This function is further integrated numerically to obtain $R_0(t)$ versus t .

All numerical calculations have been performed using Mathematica version 11.3.

[1] G. Salbreux, J. Prost, and J. F. Joanny, Phys. Rev. Lett **103**, 058102 (2009).

[2] G. F. Simmons, *Differential equations with applications and historical notes*. (CRC Press, 2016).

Supplementary Information Part-II : Dynamics and stability of the cytokinetic ring

Mainak Chatterjee, Arkya Chatterjee, Amitabha Nandi, and Anirban Sain

Department of Physics, Indian Institute of Technology-Bombay, Powai, Mumbai 400076, India

(Dated: January 26, 2022)

PACS numbers:

In the main text and Supplementary material part-1 (SI-I) we studied the contraction of the cytokinetic ring with radial symmetry as a simplifying assumption. Here, we extend the analysis to a deformed hole in order to investigate the stability of the symmetric solution derived previously. The motivation for this study arises from experimental observation about the typical shape of the ring during cytokinesis (see Fig-1 and Ref[1–3]). As shown in Fig.1, the ring contraction does not occur in a radially symmetric fashion. At the outset, the ring appears to be far from a perfect circle, but as it contracts, it becomes increasingly circular. We would like to address this observation by studying the stability of the different angular modes of the contraction dynamics. In order to make this exercise analytically tractable (in the sense of linear stability analysis), we assume small deviation from the circular shape. This is a strategy analogous to that adopted in [4] and [5] (chapter-7). By using linear stability analysis for the quasi-static ring contraction dynamics, we are able to calculate the growth/decay rate of the angular modes using perturbation theory. We find that the lowest-order breathing mode and most of the higher-order modes are stable for experimentally relevant regime of parameter values. Furthermore, for large values of ring radius, there is a window of unstable modes in between; however this window shrinks as the ring contracts and eventually all modes become stable.

We study deformations of the circular ring by decomposing into Fourier modes as modes as follows:

$$\delta R(\theta, t) = \sum_{n=0}^{\infty} \delta R_n(t) e^{in\theta} \quad (1)$$

This perturbative deformation to the ring implies that the circular ring defined by the polar equation $r(\theta) = R_0$ is now changed to $r(\theta) = R_0 + \delta R(\theta)$ (the time dependence is suppressed for simplicity of notation).

Due to this deformation, velocity and order parameter fields change perturbatively:

$$\tilde{Q}(r, \theta, t) = \tilde{Q}_0(r) + \delta \tilde{Q}(r, \theta, t) \quad (2)$$

$$q(r, \theta, t) = \delta q(r, \theta, t) \quad (3)$$

$$v_r(r, \theta, t) = v_r^0(r) + \delta v_r(r, \theta, t) \quad (4)$$

$$v_\theta(r, \theta, t) = \delta v_\theta(r, \theta, t) \quad (5)$$

The perturbation fields $\delta \tilde{Q}, \delta q, \delta v_{r,\theta}$ can be expanded

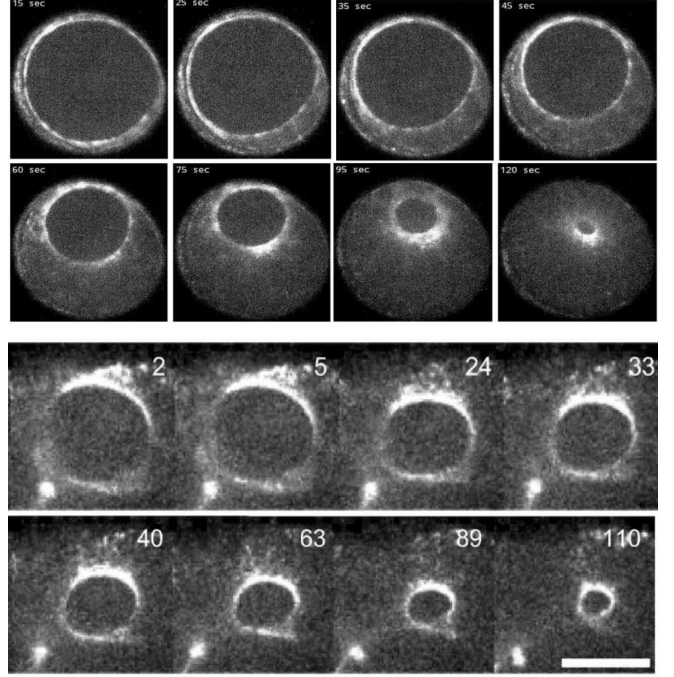


Figure 1: Experimental images of ring closure, in *c* *Elegans* cell division, adapted from different sets of experiments by Menon et al. [3] (the top two panels) and Silva et al.[2] (the 3rd and 4th panels). The scale bar is $5 \mu\text{m}$ (for the lower panel), and time is in seconds.

similar to $\delta R(\theta, t)$ as

$$\delta \tilde{Q}(r, \theta, t) = \sum_{n=0}^{\infty} \delta \tilde{Q}_n(r, t) e^{in\theta} \quad (6)$$

$$\delta q(r, \theta, t) = \sum_{n=0}^{\infty} \delta q_n(r, t) e^{in\theta} \quad (7)$$

$$\delta v_r(r, \theta, t) = \sum_{n=0}^{\infty} \delta v_{r,n}(r, t) e^{in\theta} \quad (8)$$

$$\delta v_\theta(r, \theta, t) = \sum_{n=0}^{\infty} \delta v_{\theta,n}(r, t) e^{in\theta} \quad (9)$$

We substitute these expansions in the dynamical equations and use the exact forms of the zeroth order solutions to solve for the Fourier amplitudes of all the four fields.

Dynamical equations for $\delta \tilde{Q}$ and δq — The Fourier amplitudes $\delta \tilde{Q}_n$ and δq_n of the order parameter fields

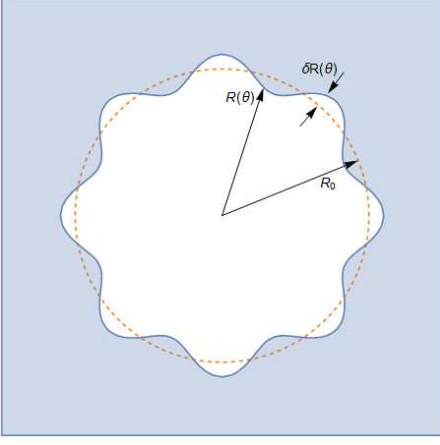


Figure 2: Deformed hole

$\delta\tilde{Q}$ and δq satisfy the following equations:

$$\left(\partial_r^2 + \frac{1}{r}\partial_r - \frac{1}{L_c^2} - \frac{n^2 + 4}{r^2}\right)\delta\tilde{Q}_n = \frac{4in}{r^2}\delta q_n \quad (10)$$

$$\left(\partial_r^2 + \frac{1}{r}\partial_r - \frac{1}{L_c^2} - \frac{n^2 + 4}{r^2}\right)\delta q_n = -\frac{4in}{r^2}\delta\tilde{Q}_n \quad (11)$$

We can diagonalise these equations by a change of variables,

$$\delta Q_+ = \delta\tilde{Q}_n + i\delta q_n \quad (12)$$

$$\delta Q_- = i\delta\tilde{Q}_n + \delta q_n \quad (13)$$

In terms of the variables δQ_+ and δQ_- , (10) and (11) give

$$\left(\partial_r^2 + \frac{1}{r}\partial_r - \frac{1}{L_c^2} - \frac{(n+2)^2}{r^2}\right)\delta Q_+ = 0 \quad (14)$$

$$\left(\partial_r^2 + \frac{1}{r}\partial_r - \frac{1}{L_c^2} - \frac{(n-2)^2}{r^2}\right)\delta Q_- = 0 \quad (15)$$

These are modified Bessel equations with solutions of the form

$$\delta Q_+ = c_n^+ K_{n+2}(r/L_c) \quad (16)$$

$$\delta Q_- = c_n^- K_{n-2}(r/L_c) \quad (17)$$

where we have left out the Bessel-I functions since δQ_\pm must go to 0 as $r \rightarrow \infty$. Changing back to $\delta\tilde{Q}_n$ and δq_n , we get

$$\delta\tilde{Q}_n = \frac{c_n^+ K_{n+2}(r/L_c) - c_n^- i K_{n-2}(r/L_c)}{2} \quad (18)$$

$$\delta q_n = \frac{c_n^- K_{n-2}(r/L_c) - i c_n^+ K_{n+2}(r/L_c)}{2} \quad (19)$$

To evaluate the constants c_n^\pm , we need to use the boundary conditions for the order parameter at the deformed ring $r = R(\theta)$,

$$\tilde{Q}(R(\theta)) = -\frac{1}{2} \quad \text{and} \quad q(R(\theta)) = \frac{1}{R_0} \frac{d\delta R}{d\theta} \quad (20)$$

By substituting (2),(3), (6) and (7) in (20), and expanding both sides to lowest order, we can obtain the following boundary conditions for the perturbation fields

$$\delta\tilde{Q}(R_0, \theta) = -\partial_r \tilde{Q}_0(R_0) \delta R(\theta) \quad (21)$$

$$\delta q(R_0, \theta) = \frac{1}{R_0} \frac{d\delta R(\theta)}{d\theta} \quad (22)$$

which imply, for the Fourier modes,

$$\delta\tilde{Q}_n(R_0) = -\partial_r \tilde{Q}_0(R_0) \delta R_n \quad (23)$$

$$\delta q_n(R_0) = \frac{in}{R_0} \delta R_n \quad (24)$$

Using these boundary conditions, we can express the exact analytical solutions for the perturbation fields $\delta\tilde{Q}_n$ and δq_n ,

$$\delta\tilde{Q}_n(r) = \frac{\delta R_n}{2R_0} \left[\left(n-1 - \frac{R_0}{2L_c} \frac{K_1(R_0/L_c)}{K_2(R_0/L_c)} \right) \frac{K_{n-2}(r/L_c)}{K_{n-2}(R_0/L_c)} - \left(n+1 + \frac{R_0}{2L_c} \frac{K_1(R_0/L_c)}{K_2(R_0/L_c)} \right) \frac{K_{n+2}(r/L_c)}{K_{n+2}(R_0/L_c)} \right] \quad (25)$$

$$\delta q_n(r) = \frac{i\delta R_n}{2R_0} \left[\left(n-1 - \frac{R_0}{2L_c} \frac{K_1(R_0/L_c)}{K_2(R_0/L_c)} \right) \frac{K_{n-2}(r/L_c)}{K_{n-2}(R_0/L_c)} + \left(n+1 + \frac{R_0}{2L_c} \frac{K_1(R_0/L_c)}{K_2(R_0/L_c)} \right) \frac{K_{n+2}(r/L_c)}{K_{n+2}(R_0/L_c)} \right] \quad (26)$$

Dynamical equations for δv_r and δv_θ — As discussed in the main text and SI-I, the velocity dynamics is expressed in terms of Navier-Stokes-like equations for the stress tensor. To perform our perturbative analysis, we

expand those equations in terms of the perturbation fields δv_r and δv_θ and then expand in terms of their Fourier modes. After some algebra, we can find the following dynamical equations for $\delta v_{r,n}$ and $\delta v_{\theta,n}$:

$$4\eta \left(\partial_r^2 + \frac{1}{r} \partial_r - \frac{4+n^2}{4r^2} \right) \delta v_{r,n} + in\eta \left(\frac{3}{r} \partial_r - \frac{5}{r^2} \right) \delta v_{\theta,n} + \zeta \Delta \mu \left[\left(\partial_r + \frac{2}{r} \right) \delta \tilde{Q}_n + \frac{in\delta q_n}{r} \right] = 0 \quad (27)$$

$$\eta \left(\partial_r^2 + \frac{1}{r} \partial_r - \frac{1+4n^2}{r^2} \right) \delta v_{\theta,n} + in\eta \left(\frac{3}{r} \partial_r + \frac{5}{r^2} \right) \delta v_{r,n} + \zeta \Delta \mu \left[\left(\partial_r + \frac{2}{r} \right) \delta q_n - \frac{in\delta \tilde{Q}_n}{r} \right] = 0 \quad (28)$$

A change of variables is needed to solve these coupled differential equations. We set $z = \ln r$ and re-write (27) and (28) as follows:

$$4 \left(\partial_z^2 - \frac{4+n^2}{4} \right) \delta v_{r,n} + 3in \left(\partial_z - \frac{5}{3} \right) \delta v_{\theta,n} = h_n(z) \quad (29)$$

$$\left(\partial_z^2 - (1+4n^2) \right) \delta v_{\theta,n} + 3in \left(\partial_z + \frac{5}{3} \right) \delta v_{r,n} = g_n(z) \quad (30)$$

where

$$h_n(z) = -\frac{\zeta \Delta \mu}{\eta} e^z \left[(\partial_z + 2) \delta \tilde{Q}_n(e^z) + in\delta q_n(e^z) \right] \quad (31)$$

$$g_n(z) = -\frac{\zeta \Delta \mu}{\eta} e^z \left[(\partial_z + 2) \delta q_n(e^z) - in\delta \tilde{Q}_n(e^z) \right] \quad (32)$$

which are functions we know exactly, in light of (25) and (26). Acting with $(\partial_z - \frac{5}{3})$ on (30), and using (29), we can eliminate $\delta v_{\theta,n}$ from these equations. Then, for modes $n \geq 2$, the solution for $\delta v_{r,n}$ is of the form

$$\delta v_{r,n} = \frac{-4+9n^2}{72n\eta} \left[\frac{C_1}{r^{n+1}} + \frac{C_2}{r^{n-1}} + C_3 r^{n-1} + C_4 r^{n+1} - \frac{1}{(n+1)r^{n+1}} \int_{R_0}^r x^n f_n(x) dx + \frac{1}{(n-1)r^{n-1}} \int_{R_0}^r x^{n-2} f_n(x) dx - \frac{r^{n-1}}{(n-1)} \int_{R_0}^r \frac{f_n(x)}{x^n} dx + \frac{r^{n+1}}{(n+1)} \int_{R_0}^r \frac{f_n(x)}{x^{n+2}} dx \right] \quad (33)$$

$f_n(x) = f_n(z)$ where $x \rightarrow e^z$ and $f_n(z) = \frac{(\partial_z^2 - (1+4n^2))}{4} h_n(z) - \frac{3in}{4} (\partial_z - \frac{5}{3}) g_n(z)$ which involves the exact solutions of $\delta \tilde{Q}_n$ and δq_n , given in (25) and (26). For the expression to not blow up at $r \rightarrow \infty$, we must enforce the following equalities:

$$C_3 = \frac{1}{(n-1)} \int_{R_0}^{\infty} \frac{f_n(x)}{x^n} dx \quad (34)$$

$$C_4 = -\frac{1}{(n+1)} \int_{R_0}^{\infty} \frac{f_n(x)}{x^{n+2}} dx \quad (35)$$

Now, to get the expression for $\delta v_{\theta,n}$, we use a simple trick. We apply $(\partial_z + \frac{5}{3})$ on (29), which allows us to derive $\partial_z^2 \delta v_{\theta,n}$. We substitute this in (30) to get an expression of $\delta v_{\theta,n}$ in terms of $\delta v_{r,n}$, $\delta \tilde{Q}_n$ and δq_n . All of this leaves us with two undetermined constants C_1 and C_2 which have to be evaluated from the stress boundary conditions which set normal component of stress tensor at $r = R(\theta)$ to 0. This implies

$$\left(\sigma_{rr} n_r + \sigma_{r\theta} n_\theta \right) \Big|_{r=R(\theta)} = 0 \quad (36)$$

$$\left(\sigma_{\theta r} n_r + \sigma_{\theta\theta} n_\theta \right) \Big|_{r=R(\theta)} = 0 \quad (37)$$

where \hat{n} is the normal vector at the deformed ring $R(\theta)$. We can evaluate \hat{n} to find:

$$\hat{n}(\theta) = -\hat{r} + \frac{1}{R_0} \frac{d\delta R}{d\theta} \hat{\theta} \quad (38)$$

where terms only up to first order in the perturbation have been kept. Hence, we can use (38) in the stress boundary conditions to obtain the following boundary conditions:

$$\delta \sigma_{rr}(R_0) = -\partial_r \sigma_{rr}^0(R_0) \delta R(\theta) \quad (39)$$

$$\delta \sigma_{\theta r}(R_0) = \frac{1}{R_0} \frac{d\delta R}{d\theta} \sigma_{\theta\theta}^0 \quad (40)$$

which implies, for the Fourier components,

$$\delta \sigma_{rr,n}(R_0) = -\partial_r \sigma_{rr}^0(R_0) \delta R_n \quad (41)$$

$$\delta \sigma_{\theta r,n}(R_0) = \frac{in}{R_0} \delta R_n \sigma_{\theta\theta}^0 \quad (42)$$

Using the above boundary conditions, C_1 and C_2 can be calculated, thereby producing the full exact solution expressed in (33).

For the modes $n = 0, 1$, the above four solutions are not independent hence these modes require a separate

analysis. In fact, for $n = 1$, a non-perturbative argument based on translation symmetry (as explained in [5]) shows that the mode should be exactly marginal i.e. $\omega_1 = 0$. For $n = 0$, however, we need to do some more work. The form of the solution for $n=0$ is:

$$\delta v_{r,0} = C_1 r + \frac{C_2}{r} + r \int_{R_0}^r \frac{g_0(x)}{x^2} dx - \frac{1}{r} \int_{R_0}^r g_0(x) dx \quad (43)$$

where $g_0(x) = -\frac{\zeta \Delta \mu}{4\eta} (\partial_r + \frac{2}{r}) \delta \tilde{Q}_0$. To prevent $\delta v_{r,0}$ from blowing up at $r \rightarrow \infty$, we must enforce

$$C_1 = - \int_{R_0}^{\infty} \frac{g_0(x)}{x^2} dx \quad (44)$$

To evaluate C_2 , we use the stress-free boundary conditions at $r = R(\theta)$ as discussed already. This gives us the full solution for $\delta v_{r,0}$. The rest of the analysis can be continued as for other modes.

Kinematic boundary condition — We define the ring velocity $V(\theta) = (v_r \hat{r} + v_\theta \hat{\theta}) \cdot \hat{n} \Big|_{R(\theta)}$, where $R(\theta) = R_0 + \delta R(\theta)$. Splitting \vec{v} into zeroth order solution and perturbation, we find:

$$\begin{aligned} V(\theta) &= (v_r^0(r) \hat{r} + \delta v_r(r, \theta) \hat{r} + \delta v_\theta(r, \theta) \hat{\theta}) \cdot \hat{n} \Big|_{R(\theta)} \\ &= -v_r^0(R) - \delta v_r(R) - \frac{\delta v_\theta(R)}{R_0} \frac{d\delta R}{d\theta} \\ &\approx -(v_r^0(R_0) + \partial_r v_r^0(R_0) \delta R(\theta)) - \delta v_r(R_0, \theta) \\ \therefore \delta V(\theta) &\equiv V(\theta) - (-v_r^0(R_0)) \\ &= -\partial_r v_r^0(R_0) \delta R(\theta) - \delta v_r(R_0, \theta) \end{aligned} \quad (45)$$

Converting to Fourier modes again, with $\delta V_n = \frac{1}{2\pi} \int_0^{2\pi} \delta V(\theta) e^{-in\theta}$, we have:

$$\delta V_n = -\partial_r v_r^0(R_0) \delta R_n - \delta v_{r,n}(R_0) \quad (46)$$

We now need to set up a kinematic boundary condition. This relates δV to δR as:

$$\delta V_n = -\frac{d\delta R_n}{dt} \quad (47)$$

which gives us a way to evaluate ω_n - the growth/decay rate of the n th Fourier mode. The time dependence of the Fourier modes can be put in as follows:

$$\delta R(\theta, t) = \sum_{n=0}^{\infty} \delta R_n e^{in\theta + \omega_n t} \quad (48)$$

Therefore, $\frac{d\delta R_n}{dt} = \omega_n \delta R_n$. So we derive, from (47),

$$\omega_n = \partial_r v_r^0(R_0) + \frac{\delta v_{r,n}(R_0)}{\delta R_n} \quad (49)$$

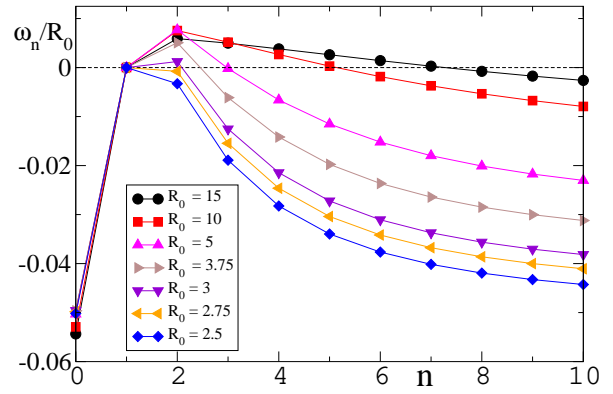


Figure 3: ω_n/R_0 versus n for different values of R_0 . The units of length and time are $L_c \simeq 1\mu m$ and $\frac{\eta}{\zeta \Delta \mu} \simeq 2sec$, respectively.

We performed the calculation outlined above on Mathematica, choosing a set of parameter values that are experimentally relevant (given in main text). We have plotted ω_n as a function of mode number n . We find that the unstable modes are present in a small window for large values of the dimensionless radius R_0/L_c . As the ring radius becomes smaller, the window of instability slowly diminishes in size and finally, at small enough radius, there are no unstable modes left. This parallels the experimental observation that asymmetrical modes are prominent when the contracting ring is large but they essentially disappear when the ring contracts to a small size, turning it into an increasingly perfect circle.

-
- [1] A. S. Maddox, L. Lewellyn, A. Desai, and K. Oegema, Developmental cell 12, 827 (2007).
 - [2] A. M. Silva, D. S. Osório, A. J. Pereira, H. Maiato, I. M. Pinto, B. Rubinstein, R. Gassmann, I. A. Telley, and A. X. Carvalho, , Journal of Cell Biology 215, 789 (2016).
 - [3] V. V. Menon, S. Soumya, A. Agarwal, S. R. Naganathan, M. M. Inamdar, and A. Sain, Biophysical journal 113, 2787 (2017).
 - [4] C. Pérez-González, R. Alert, C. Blanch-Mercader, M. Gómez-González, T. Kolodziej, E. Bazellieres, J. Casademunt, and X. Trepat, Nature physics 15, 79 (2019).
 - [5] R. A. Zenón, PhD dissertation, Universitat de Barcelona (2018).